ELSEVIER

Contents lists available at ScienceDirect

Journal of Archaeological Science: Reports

journal homepage: www.elsevier.com/locate/jasrep



Archaeomagnetic dating of vitrified Broborg hillfort in southeast Uppsala, Sweden



Mostafa Ahmadzadeh^a, Cristina García-Lasanta^b, Bernard Housen^b, John S. McCloy^{a,c,*}

- ^a Materials Science and Engineering Program, Washington State University, Pullman, WA 99164, USA
- ^b Geology Department, Western Washington University, Bellingham, WA 98225, USA
- ^c Department of Mechanical and Materials Engineering, Washington State University, Pullman, WA 99164, USA

ARTICLE INFO

Keywords: Sweden Hillfort Archaeomagnetic dating Paleodirection Paleointensity Iron Age

ABSTRACT

Hundreds of European hillforts from the Bronze and Iron Ages show evidence of extreme heating of the stone ramparts, which has caused melting of the rocks which partially turned to glass on cooling. The cause and age of wall vitrification at these hillforts has long been debated in the archaeological community. This work aims to determine the age of vitrification at the Broborg hillfort (Uppsala, Sweden) using archaeomagnetic dating. Rock magnetic investigations verified the suitability of the vitrified materials for such studies, with titanomagnetites being the major magnetic signal carriers. Despite the challenges involved in sample collection at the Broborg site, a total of eight oriented samples (five vitrified, three non-vitrified) were collected and used in this study. The mean paleodirection and paleointensity results were combined to compare with a geomagnetic field model for Europe. Three possible archaeomagnetic age intervals for Broborg vitrification were found: 389–579 CE, 602–752 CE, and 965–1300 CE, among which the 389–579 CE date range is the most consistent with the published ¹⁴C ages and known historical context of the site. This study shows that paleointensity data alone could be used to date such sites, requiring smaller unoriented samples, potentially removing some of the barriers to sample acquisition at some archaeological sites.

1. Introduction

A hillfort is a type of prehistoric fortification consisting of one or more lines of earth or stonework (fort), on a raised area of land (hill). These structures are typically thought to have been constructed for defensive purposes, though other uses have been suggested (Harding, 2012; Ralston, 2013). Some hillforts are known with portions of stone ramparts which have clearly been exposed to high enough temperatures to partially melt some of the rocks that make up the walls, which then vitrified (turned to glass, or fine-grained aphanitic rock) upon cooling. > 130 vitrified forts are identified in Europe dating as early as the Late Bronze Age, with most of these tentatively dated to the Iron Age (c. 1000 BCE - 1000 CE) (Berrocal-Rangel et al., 2019; Kresten et al., 1993; Kresten and Kresten, 1996; Sanderson et al., 1985). Vitrified hillforts in Scotland are the most well studied (Cotton, 1954; Ralston, 2013; Sanderson et al., 1985), yet many other sites are known from places such as France (Vernioles, 2013), Sweden (Kresten and Ambrosiani, 1992), Germany (Röpke and Dietl, 2014), and Portugal (Berrocal-Rangel et al., 2019; Catanzariti et al., 2008).

Debate about the cause of wall vitrification at sites such as these is

as old as the historical writing about them (Russell, 1894). Archaeological interpretation ranges from destruction by enemy fire (Cotton, 1954; Harding, 2012; Kresten, 2004; Ralston, 1986) to lightning (Kresten and Ambrosiani, 1992) to constructive mechanical enhancement (Brothwell et al., 1974; Youngblood et al., 1978) to unspecified ritual purpose (Vernioles, 2013). There is at least some evidence for all of these explanations, and the cause (and purpose) of the vitrification almost certainly differs from site to site (Kresten and Ambrosiani, 1992). Better constraints on the age of the vitrified material in these sites, by documentation of possible variations in age(s) within a site and for the overall range of ages of vitrified hillforts within a region, can help to better understand the origin and cultural context of these distinctive features.

Broborg hillfort, which is located about 20 km southeast of Uppsala, Sweden (17.9515°E, 59.7556°N), is one of the well-known structures with prevalent wall vitrification identified in Sweden (Kresten et al., 1993). Broborg has a halfmoon-shaped structure with dry-laid outer ramparts built from moraine boulders on top of a hill; these extant 'walls' rise to about 2 m high and 4–6 m thick. The inner rampart is similarly constructed, but additionally shows signs of extensive

^{*} Corresponding author at: Materials Science and Engineering Program, Washington State University, Pullman, WA 99164, USA. E-mail address: john.mccloy@wsu.edu (J.S. McCloy).

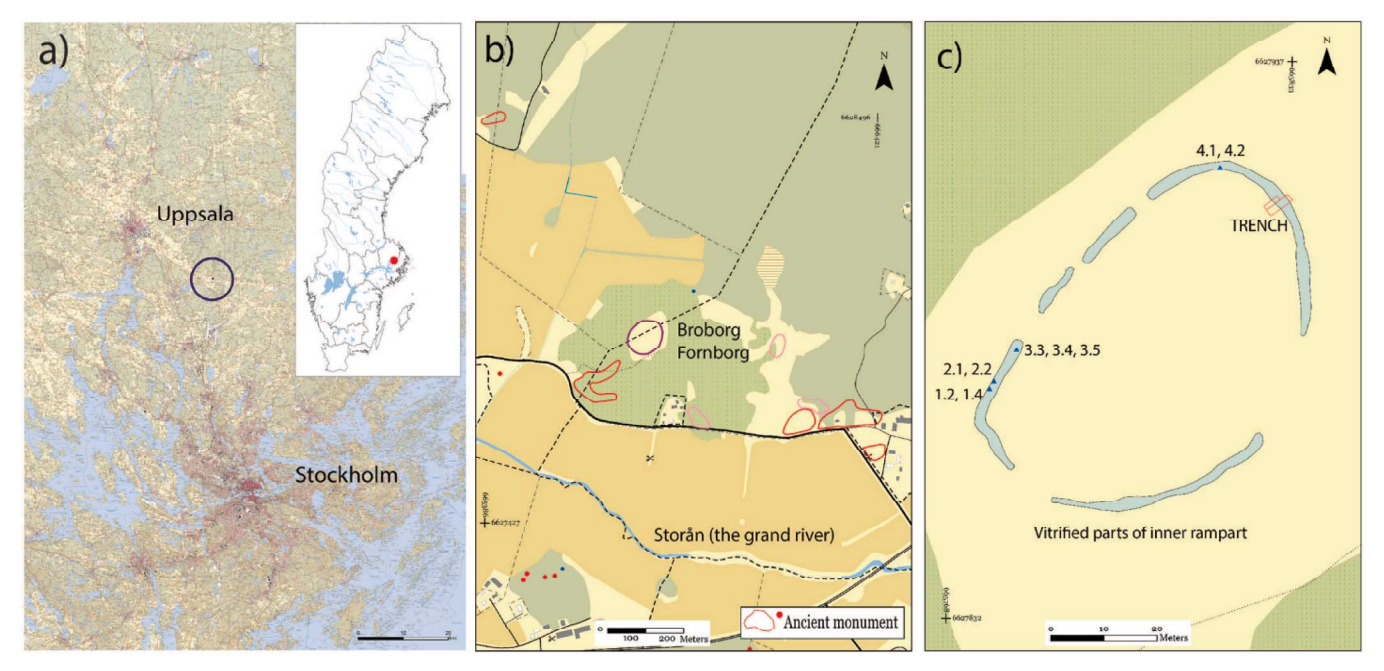


Fig. 1. Maps of Broborg: a) area of Broborg site (circled) with respect to major Swedish cities, also showing overall location in Sweden (inset); b) local map roughly corresponding to the circle in a), showing of Broborg fornborg (hillfort) near the center of the map; for more details on the named nearby ancient monuments, see Fig. S.1. in Supplementary Material; c) Broborg hillfort site map showing vitrified inner rampart areas (blue), along with sites where drill samples were obtained (triangles), as well as trench excavation (rectangles). Courtesy of Mia Englund and Archaeologerna (The State Archaeologists, Sweden).

vitrification in various areas, which can be distinguished by the smooth topography of the top-most surface of the wall. The building materials of the walls are mainly granitic gneiss and amphibolite (Kresten et al., 1993). Recently a fine-grained basaltic dike (dolerite/diabase) was discovered on the Broborg hill, which may be another possible source of mafic material for the wall (Englund, 2018). The aphanitic, vesicle-rich, black melt-products derived from melted wall-rock source material can be observed in the vitrified sections of these walls. Additionally, a transparent-to-white superficial melt is often also observed, and has been described as the 'clear glass' as distinct from the 'opaque or black glass' (Kresten and Ambrosiani, 1992; Weaver et al., 2018).

There is strong evidence that high temperatures (> 700 °C but possibly as high as 1100 °C in places) must have been reached for significant amounts of time (hours to days) in order to melt these rocks (Kresten et al., 1993). Melting of probable source materials (amphibolite or dolerite or felsic gneiss) has been shown to produce magnetite (and related spinel phases) or occasionally hematite on cooling (Kresten et al., 1993; Yoder and Tilley, 1962). Either type of Fe-containing mineral would record the geomagnetic field present at the site during cooling below the Curie or Néel temperature of the specific magnetic mineral formed in the melt product. This magnetic recording will occur even if hematite or magnetite was present in the original rock and was heated above the Curie/Néel temperature without melting. For the Broborg site, Kresten and Ambrosiani (1992) have reported that the vitrified areas have higher magnetic susceptibility than surrounding wall materials, which they attribute to formation of magnetic minerals in the melt as described above. Therefore, the Fe-oxide (magnetite or hematite) particles formed at the time of the rock partial melting followed by vitrification can be a promising source for archaeomagnetic dating of the melting event, interpreted archaeologically at Broborg as being related to the site construction. Archaeomagnetic dating can be performed by comparing the direction and intensity of the thermoremnant magnetization (TRM) with a regional reference of the geomagnetic field.

There have been a few studies on archaeomagnetic dating of vitrified forts in Europe. Gentles and Tarling (1993) successfully dated six Scottish prehistoric vitrified structures employing directional

archaeomagnetic techniques, with details discussed in Gentles (1989). They found the vitrification dates of their studied forts to lie within the range of 300 BCE - 500 CE, which was claimed to be in good agreement with the radiocarbon dating results. Clelland (2011) discussed the results of various attempts to date British vitrified hillforts. It was pointed out in her work that, given the differences in the recorded TRM signals, it is unlikely that the Scottish forts were all vitrified within a relatively short period of time. Catanzariti et al. (2008) performed archaeomagnetic dating for a vitrified wall at the Misericordia site in Portugal by comparing the TRM direction with a reference secular variation curve suitable for the site location. It was found that vitrification at Misericordia occurred 842-652 BCE, corresponding to the Late Bronze Age occupation period. Their study also yielded promising results supporting the suitability of such techniques for dating vitrified structures. Finally, a single directional measurement has been reported from Camp de Péran hillfort in France, which was paleomagnetically dated to 915 \pm 20 CE (Vernioles, 2013). Thus, there is suggestion that these forts were vitrified over a thousand-year period in different regions. Additional work to include estimates of the geomagnetic field intensity as well as direction, and other archaeological and dating evidence to constrain the likely time of crystallization of the primary TRM carriers, can be used to more precisely determine the age of these hillfort vitrification events at these sites.

Dates for the Broborg site have been obtained from various techniques and summarized (Englund, 2018; Kresten et al., 1993). A posthole inside the rampart is dated by $^{14}\mathrm{C}$ to 446 CE (430–660 CE, one sigma). A glass bead found inside the fort in the 1980s has unclear archaeological context but has been classified as Petré P5-type (ca. 700 CE) by Upplandsmuseet (Fagerlund, 2009). Thermoluminescence (TL) of burnt stones under the vitrified layer gives a date of 740 \pm 100 CE; however, considerable difficulties with TL have been pointed out for fire-cracked stones and high temperature fired materials (Catanzariti et al., 2008; Kresten et al., 2003). To the authors' knowledge, no published attempts have been made to date Broborg's vitrification by comparing the paleomagnetic signal recorded by the melt products with regional compilations and models for paleosecular variation. In the present work, suitability of the archeological vitrified materials at

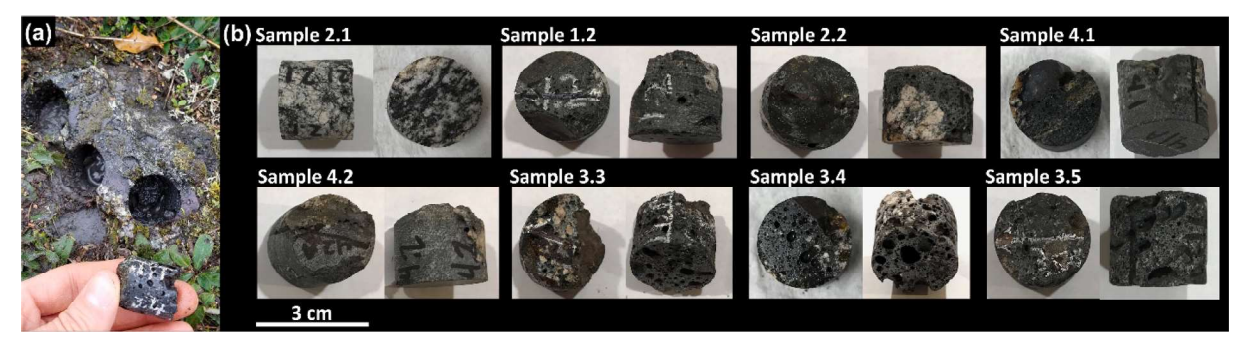


Fig. 2. a) drilled oriented sample with apparent signs of extensive vitrification throughout the entire sample (sample 3.4), and b) all eight oriented samples cut for directional measurements.

Broborg for paleomagnetism, as well as the nature and stability of the magnetic carriers, are investigated using rock magnetic techniques. The results from both paleomagnetic directions as well as paleointensity of primary remanence (here referred to as natural remanent magnetization or NRM) measurements are reported, and age constraints obtained by archaeomagnetic dating is discussed.

2. Sampling and methods

The location of Broborg with respect to Sweden and the local area around Uppsala is shown in Fig. 1a and b, respectively.

Archaeological samples were mostly collected from the vitrified sections (black porous rocks) for standard rock magnetic, paleodirection, and paleointensity measurements. Locations for the collected samples used in this study with respect to Broborg hillfort are shown in Fig. 1c. The Broborg vitrified materials are normally highly vesicular, brittle, and often heterogeneous. Moreover, in most places, the molten layer is only a thin superficial coating on wall rocks. Consequently, collecting vitrified oriented samples was especially difficult at Broborg, and sample length was very limited. Fig. 2a shows one of the successfully drilled samples with extensive vitrification throughout the entire sample. A total of eight cylindrical samples with the standard dimensions for paleomagnetic studies (2.5 cm diameter) were successfully drilled out of the walls with a gas-powered diamond-tipped portable drill and oriented using a magnetic compass: one granitic gneiss (2.1), two mostly vitrified vesicular samples (1.2 and 2.2), two 'non-vitrified' samples with superficial melting (4.1 and 4.2), and three samples from vitrified highly vesicular material (3.3, 3.4, 3.5). All oriented samples are shown in Fig. 2b. An unoriented block of black rock (sample 1.4) with signs of heating/melting was also collected and used for basic rock magnetic experiments. Use of a secondary solar compass was not possible due to weather, but field experiments suggested that magnetic compass measurements should be reliable. All oriented samples were cut into standard 2.2 cm long specimens, using a brass saw with water circulation, with one to two specimens obtained from each sample.

For the rock magnetic measurements, three vitrified pieces (of unoriented sample 1.4) with masses \sim 100-300 mg were used. Room temperature magnetic hysteresis loops and first order reversal curves (FORCs) were obtained using a vibrating sample magnetometer (VSM, PMC3900, Lakeshore Cryotronics, Westerville, OH) with maximum applied field of 1.8 T. In order to identify minerals, magnetic susceptibility as a function of temperature was measured with a susceptometer (KLY3 Kappabridge, AGICO Inc., Czech Republic) equipped with devices to control temperature changes (CS-L and CS-3 for low and high temperatures, respectively). Three sub-samples of powered material from the unoriented block sample 1.4 were used for these measurements. Liquid nitrogen was used for the low-temperature measurements from -190 to 0 °C, while high-temperature measurements were performed from room temperature to 700 °C on both heating and cooling, all under Ar flow in order to minimize mineral neoformations associated with heating during the experiment.

All collected oriented samples were subjected to a progressive alternating-field (AF) demagnetization employing an AF demagnetizer (D-Tech D-2000, ASC Scientific, USA), followed by magnetization measurements using a dual speed spinner magnetometer (JR-6A, AGICO Inc., Czech Republic). All the procedures were performed inside the shielded room available at the Pacific Northwest Paleomagnetism Laboratory (PNwPL) at Western Washington University (WWU). The samples were demagnetized in 13 steps with demagnetization field peaks ranging between 5 and 140 mT in increasing intervals from 5 to 20 mT (for lower and larger peak fields, respectively). Orthogonal vector diagrams (Zijderveld, 1967) and equal-area projections were plotted to discuss the AF demagnetization data. Principal component analysis (PCA) (Kirschvink, 1980) was used to calculate the paleomagnetic directions on the orthogonal diagrams, using both PuffinPlot (Lurcock and Wilson, 2012) and IAPD (Torsvik et al., 2000) software.

Twelve representative chips (between 198.6 mg and 1479.3 mg in weight) were collected from the drilled samples (one or two from each

 Table 1

 Characteristic components for the studied samples.

Field Sample ID	Archaeologists' GPS ID (Fig. 1)	Sample description	Primary remanence intensity (mA/m)	PCA fit range (mT)	Dec (°)	Inc (°)	MAD
1.2ª	P591	Vesicular vitrified	0.216	60–140	000.7	79.5	2.2
1.4 ^b	P593	Vesicular vitrified	N/A	N/A	N/A	N/A	N/A
2.1	P602	Granite	0.050	40-80	346.7	79.4	1.2
2.2 ^a	P603	Vesicular vitrified with molten top and a granitic inclusion	0.324	60–140	30.1	81	2.2
3.3 ^a	P626	Highly vesicular vitrified	0.128	70-140	25.3	70.9	2.9
3.4 ^a	P627	Highly vesicular vitrified	0.184	60-140	11.4	68.9	1.2
3.5 ^a	P628	Highly vesicular vitrified	0.257	60-140	25.3	70.9	0.8
4.1	P623	Non-vitrified with vitrified top	0.169	60-140	302.3	74.2	1.2
4.2	P624	Non-vitrified	0.365	60–140	285.3	64.4	2.1

^a Used in mean direction determination to compare with geomagnetic field models.

^b Unoriented sample used for basic rock magnetic measurements.

 Table 2

 Estimated paleofield intensity and error for each sub-sample (see text for details).

Collected sample	Sub-sample	T range (°C)	Raw calc Int (µT)	error	class	pTRM check co Int (μT)	orrected calc. error	class
1.2	B1-2A	325–510	62.5	2.1	а	N/A		
	B1-2B	230-505	67.7	1.9	c	69.8	2.8	\boldsymbol{A}
2.2	B2-2A	370-450	63.9	0.6	а	N/A		
3.3	B3-3A	200-530	<i>7</i> 3.9	3.9	а	N/A		
	B3-3B	230-530	77.6	9.8	c	66.8	3.1	B
3.4	B3-4A	300-490	<i>57.9</i>	2.7	а			
	B3-4B	230-505	75.2	3.4	b	69.2	3.6	B
3.5	B3-5A	250-530	<i>79.7</i>	3.4	а	N/A		
4.1	B4-1A	300-530	69.2	2.8	b	N/A		
	B4-1B	325-480	66.3	2.3	c	53.4	2.7	Α
4.2*	B4-2A	300-490	95.44	9.9	b	N/A		
	B4-2B	120-410	67.6	2.6	b	63.0	6.3	В
Mean*	Set A		67.8	7.3		N/A		
Mean	Set B		70.9	4.6		64.4	6.0	
Mean*	All		69.2	6.4				
Mean	See discussion	Int: 67.9 μ T; error: 6.4 μ T						

*Sub-sample B4.2A is not included in the mean values (see text for details).

of the oriented samples denoted in Table 1 except 2.1; see Table 2 for further details) and subjected to a Thellier-type protocol (Thellier and Thellier 1959), following the variations suggested by Coe (1967). These analyses were also performed in the shielded room available in the PNwPL at WWU, with the aim to describe the absolute paleointensity of the primary remanence by reproducing their TRM in the laboratory, which is the mechanism of remanence acquisition expected in the studied materials (Catanzariti et al., 2008; Clelland, 2011). Two sets of samples were used in these experiments.

An initial set of seven chips (labeled as "A" on Table 2) of vitrified material were treated with a total of 14 double heating–cooling steps (from 100 °C to 510 °C; temperatures > 510 °C were not required as remanence was nearly or fully removed). These steps were performed within a paleomagnetic oven (TD48 SC, ASC Scientific, USA) under a controlled Ar atmosphere. The first of each double step was performed under zero field conditions, whereas the second was performed under a 40 μT field (Coe, 1967). For this first set of results, pTRM checks were not conducted.

A second set of experiments included five additional chips of vitrified material (labeled as "B" on Table 2). These were subjected to 13 double heating-cooling steps (from 120 °C to 530 °C; temperatures > 530 °C were not required as remanence was nearly or fully removed), six pTRM checks to evaluate for alterations associated to heating (Thellier and Thellier 1959) distributed every other temperature increase, starting after 290 °C with a check at 230 °C, and three pTRM tail checks performed right before every other pTRM check. These tail checks were performed in order to test for the multidomain (MD)

content in the studied materials (Riisager and Riisager, 2001).

Each sample chip was placed in an individual flat rounded Pyrex glass that was oriented, in order to ensure the same position was arranged within the oven in every temperature cycle (and thus with respect to the applied field). The remanent magnetization of each sample was measured in each step using the same spinner magnetometer mentioned above. In order to use the magnetometer standard holder, the glass-chips assemblages were mounted on cylindrical, standard-size plastic holders. The signal of each plastic holder was subtracted individually prior to each measuring step. The resultant partial TRM (pTRM) data were plotted and analyzed with ThellierTool software (Leonhardt et al., 2004).

After the AF demagnetization process mentioned above was completed, four of the most representative samples (2.1, 4.1, 2.2, and 3.3) were thin-sectioned and observed by optical microscopy (see Figs. S.2.1-S.2.4 in Supplementary Material). Cut sections of the same samples were ground and used for powder X-ray diffraction analysis (XRD, see Fig. S.3.). In addition, electron microprobe analysis (EPMA) was performed on samples 3.3 (highly vesicular vitrified) and 2.2 (vesicular vitrified with molten top and a granitic inclusion) using a JEOL JXA-8500F (see Section S4 in Supplementary Material for details).

3. Results

3.1. Mineralogy

As revealed by the XRD results (Fig. S.3), the granitic sample (2.1) is

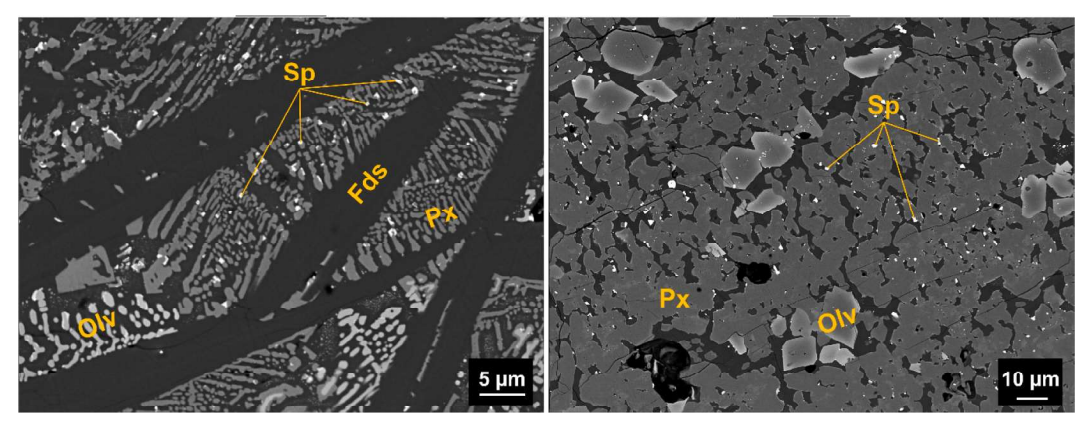


Fig. 3. BSE images of one of the samples with extensive vitrification (sample 3.3), showing iron spinel (Sp), pyroxene (Px), feldspar (Fds), and olivine (Olv) phases. These phases were identified, and their composition was measured using electron microprobe (see Section S4 on Supplementary Material).

mostly composed of quartz with considerable fractions of feldspars (anorthoclase and sanidine). The other three representative samples (4.1, 2.2, and 3.3; Fig. 3) exhibit similar mineralogy including different fractions of plagioclase (andesine), clinopyroxene (augite), olivine (ferroan forsterite), spinel (magnetite), and quartz. Note that the iron spinel phase can have different compositions that are difficult to distinguish in XRD due to small compositional variation. The assignments to particular minerals from XRD results are broadly consistent with the microprobe measurements (see below) taken on samples 3.3 and 2.2.The fractions of each crystalline phase, as calculated by Rietveld refinement, are provided in the Section S.3 in Supplementary Material.

Back-scattered electron (BSE) images of a highly-vitrified sample (sample 3.3 as a representative sample, Fig. 3) were also obtained, particularly to examine the size and morphology of the magnetic minerals. Despite the presence of some larger, likely relict, iron oxide grains (See Section S.4 in Supplementary Material), desirably-small magnetite particles were observed in the microstructure. The BSE images in Fig. 3 show that $\sim 1~\mu m$ spinel particles crystallized mostly within the clinopyroxenes (augite), likely on cooling during the vitrification, as they are not present in the microstructures of candidate source rocks. Such particles are the promising carriers of the geomagnetic field at the time of vitrification.

All five phases detected by XRD were successfully identified in microprobe analysis of sample 3.3. WDS quantitative point analysis of the four phases (except quartz) was performed and is detailed in the Supplementary Material. The average compositions of the measured phases are as following (for more accurate average compositions see Tables S.4.1-S.4.4): i) clinopyroxene ($Ca_{0.8}Mg_{1.0}Fe_{0.2}$)($Al_{0.1}Si_{1.9}$)O₆ (normalized to 6 oxygens), while the concentration of Ca, Mg, and Fe varies; ii) olivine $Mg_{1.4}Fe_{0.6}SiO_4$ (normalized to 4 oxygens), while the concentration of Mg and Fe varies; and iii) plagioclase feldspar ($Na_{0.4}Ca_{0.6}$)($Al_{1.4}Si_{2.6}$)O₈ (normalized to 8 oxygens).

Most of the spinel grains were too small to measure, though a few larger grains were measured for their composition. Both ${\rm Fe}^{2+}$ and ${\rm Fe}^{3+}$ are present in the spinel phase, and it is not possible to measure analytically the concentration of each one in microprobe. However, the ${\rm Fe}^{2+}$ and ${\rm Fe}^{3+}$ was calculated through cation normalization (Deer et al., 1992), which provides an estimated spinel composition of ${\rm Fe}_{2,4}{\rm Ti}_{0.3}{\rm Mg}_{0.1}{\rm Al}_{0.17}{\rm O}_4$. For comparison with measured magnetization of the spinels (see below), the Ti content taken in isolation would suggest a Tm30 (${\rm Fe}_{2,7}{\rm Ti}_{0.3}{\rm O}_4$) composition. If the non-Fe cations are added to the Ti as substitutions for Fe in the spinel lattice, the composition of this spinel would be ${\rm Fe}_{2,4}{\rm Ti}_{0.6}{\rm O}_4$, corresponding to a \sim Tm60 titanomagnetite composition.

3.2. Rock magnetism

The thermomagnetic results (normalized magnetic susceptibility versus temperature) of the glassy vitrified unoriented sample 1.4 as generally representative are shown in Fig. 4a. The results reveal a reversible behavior of the heating and cooling runs and significant magnetic susceptibility increase along the temperature range associated to the Verwey transition (Verwey, 1939) for the low-temperature segment of the curve and a drop in magnetic susceptibility at $\sim 300\text{--}450\,^{\circ}\text{C}$ for the high-temperature heating segment. Such results point to the presence of one population of homogenous titanomagnetite. According to the data summarized by Lattard et al. (2006), synthetic titanomagnetite composition (Fe(3-x)Ti_xO_4) with x ~ 0.3 shows the same T_C . This is consistent with the x ~ 0.3 (Tm30) composition estimated from the EMPA data, with unknown complications in the T_C due to significant Al and Mg substitution. The sample shows a narrow hysteresis behavior (Fig. 4b) with $H_C=8$ mT and $M_S=2.49$ Am²/kg.

The FORC diagram of the same sample is presented in Fig. 4c. The diagram was generated using FORCinel software (Harrison and Feinberg, 2008) (V2.05 in IGOR Pro6, WaveMetrics, Portland, OR), with smoothing factor 3, the optimum calculated by the software. The

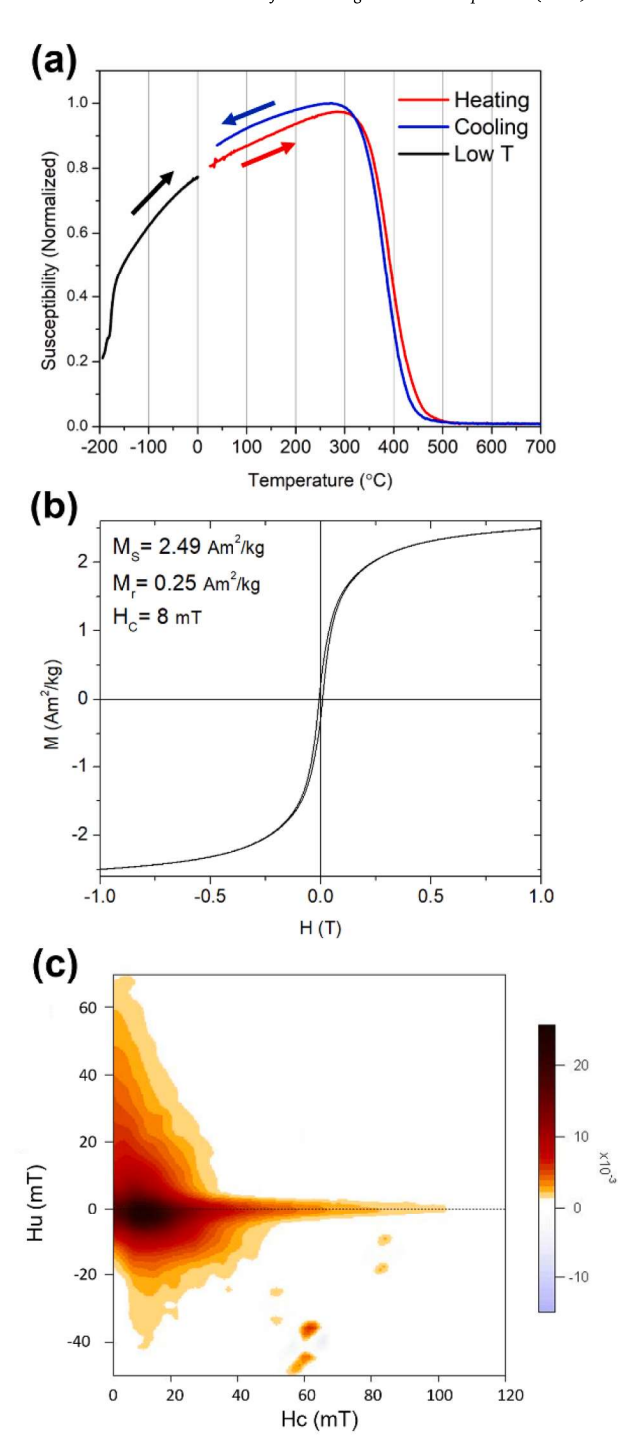


Fig. 4. Rock magnetic measurement results of a vitrified Broborg hillfort sample (sample 1.4a), a) suceptibility versus temperature, b) magnetic hysteresis curve, and c) FORC diagram.

FORC diagram shows the main peak (center of the contours) at $H_{\rm C} \sim 10$ mT, which is consistent with the coercivity obtained from the hysteresis loop. It also shows a tail at higher coercivities, which could be due to smaller population of magnetic grains with different sizes. The FORC diagram suggests magnetic vortex states (i.e., pseudo-single-domain (PSD) behavior) due to grain sizes larger than single domain magnetite (i.e., $>75\,$ nm), with some significant magnetic interaction between states (Roberts et al., 2017). The rock magnetic results of the vitrified Broborg sample, as a representative sample, show promise for paleomagnetic recording of the past Earth's magnetic field.

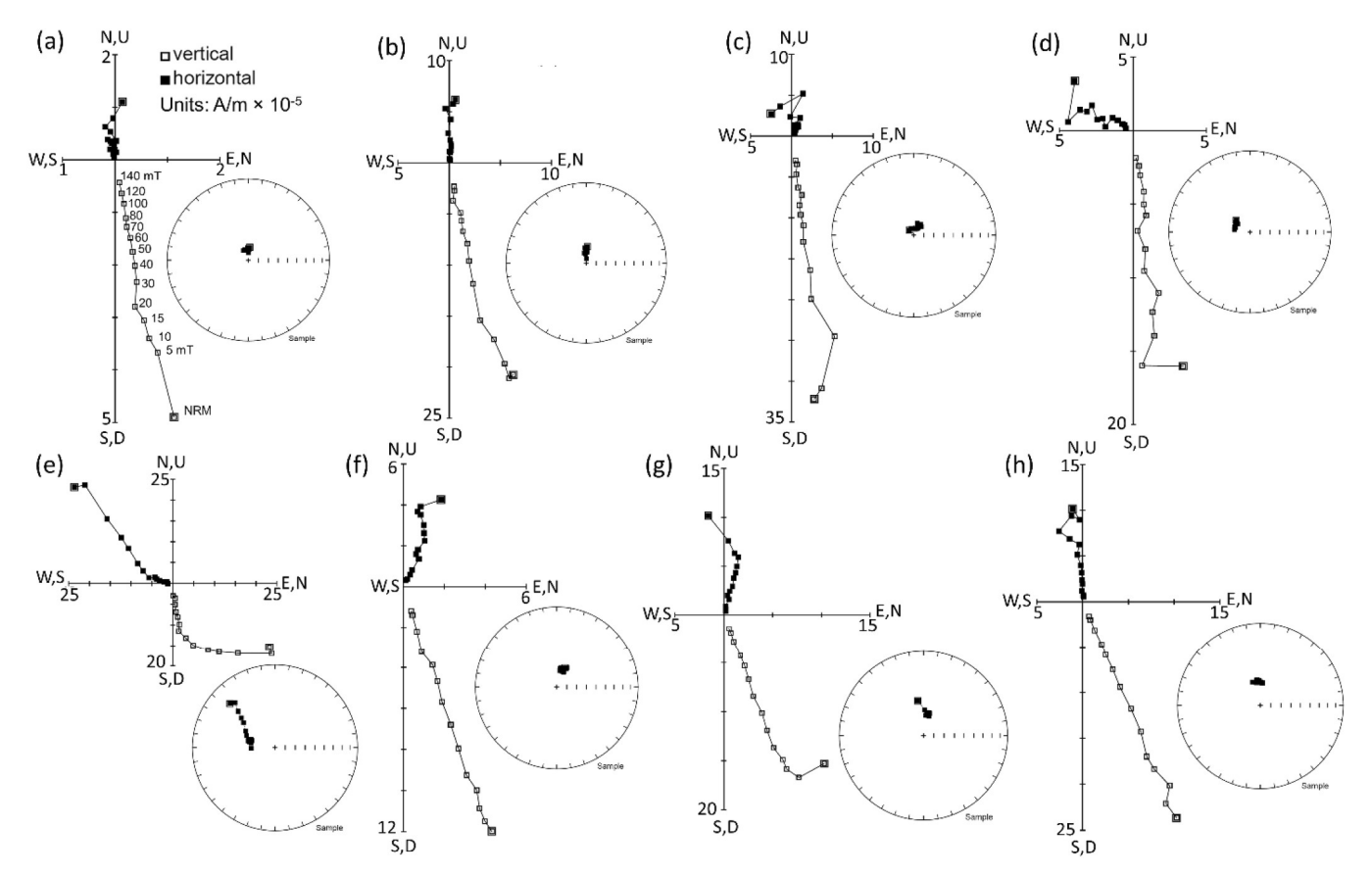


Fig. 5. Stepwise AF demagnetization diagrams; orthogonal projections and equal-area plots of eight oriented Broborg samples: a) 2.1 (gran., heated), b) 1.2 (vitrif.), c) 2.2 (vitrif.), d) 4.1 (heated), e) 4.2 (non-h.), f) 3.3 (vitrif.), g) 3.4 (vitrif.), and h) 3.5 (vitrif.). Open squares are the vertical magnetization component and filled squares the horizontal component. Abbreviations for samples are gran. (granite), vitrif. (vitrified), non-h. (non-heated).

3.3. Paleodirection

Table 1 lists the oriented samples studied using stepwise AF demagnetization experiments with the measured intensity, along with their declination and inclination calculated by PCA. Fig. 5 presents the orthogonal and equal-area projections for these samples. Most of the samples behaved similarly during AF demagnetization. > 90% of the primary remanence is demagnetized at the peak applied AF of 140 mT for all samples. With the exception of sample 4.2 (Fig. 5e), the other samples show a single component of remanent magnetization which stabilizes towards the center of the orthogonal plot at AF > 10 mT. The results from sample 4.2 show two components of magnetization, and the direction of this sample was obtained after removing the second component. For all specimens, the characteristic component was well-defined, with a maximum angular deviation (MAD) for the PCA line fit of less than 3°. The directions are given in Table 1 and plotted in Fig. 6.

In order to obtain the mean direction, the directions of all eight oriented samples can be considered together (Fig. 6a), or separated into groups that combine petrographic texture and their magnetic directions. The directions from the five most vitrified samples (i.e., 1.2, 2.2, 3.3, 3.4, and 3.5) shown in Fig. 6b cluster together and have a mean direction of D = 11.3°, I = 73.7°, N = 5, k = 115, α_{95} = 7.2°; here D and I are declination and inclination, respectively; N is the number of samples; k is the Fisher precision parameter (Fisher, 1953); and α_{95} is the radius of the cone at 95% level of confidence around the mean direction. The granitic (2.1) and the non-vitrified with molten top (4.1) samples also have directions that are similar to those of the vitrified samples – these are referred to as 'heated' samples. The mean direction of combined vitrified and heated samples is D = 360°, I = 75.9°, N = 7, k = 76, α_{95} = 7° (Fig. 6c). However, the mean direction of the

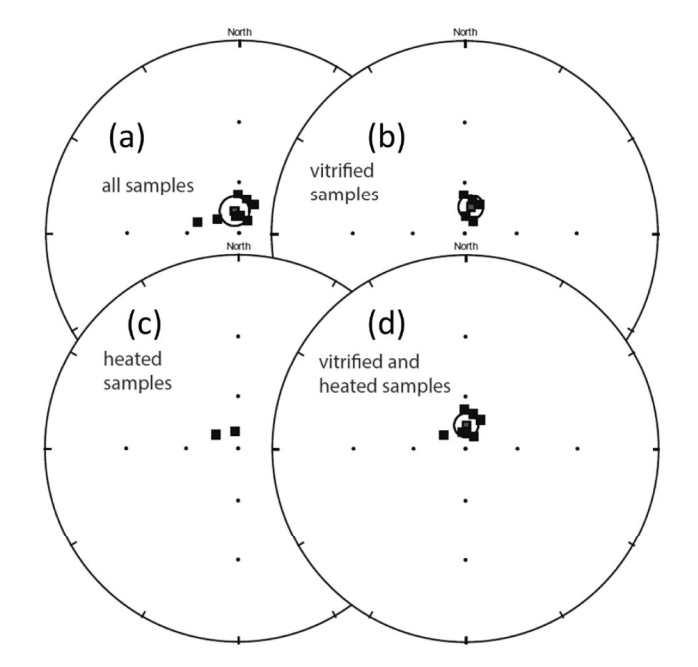


Fig. 6. Equal-angle projections of the mean directions for the studied oriented samples in various groups; a) all eight studied oriented samples, b) five most vitrified samples (1.2, 2.2, 3.3, 3.4, and 3.5), c) heated samples (2.1 and 4.1) with relatively close mean directions to those of vitrified ones, and d) vitrified group and heated group. Vitrified group (b) was used for comparison to geomagnetic field models.

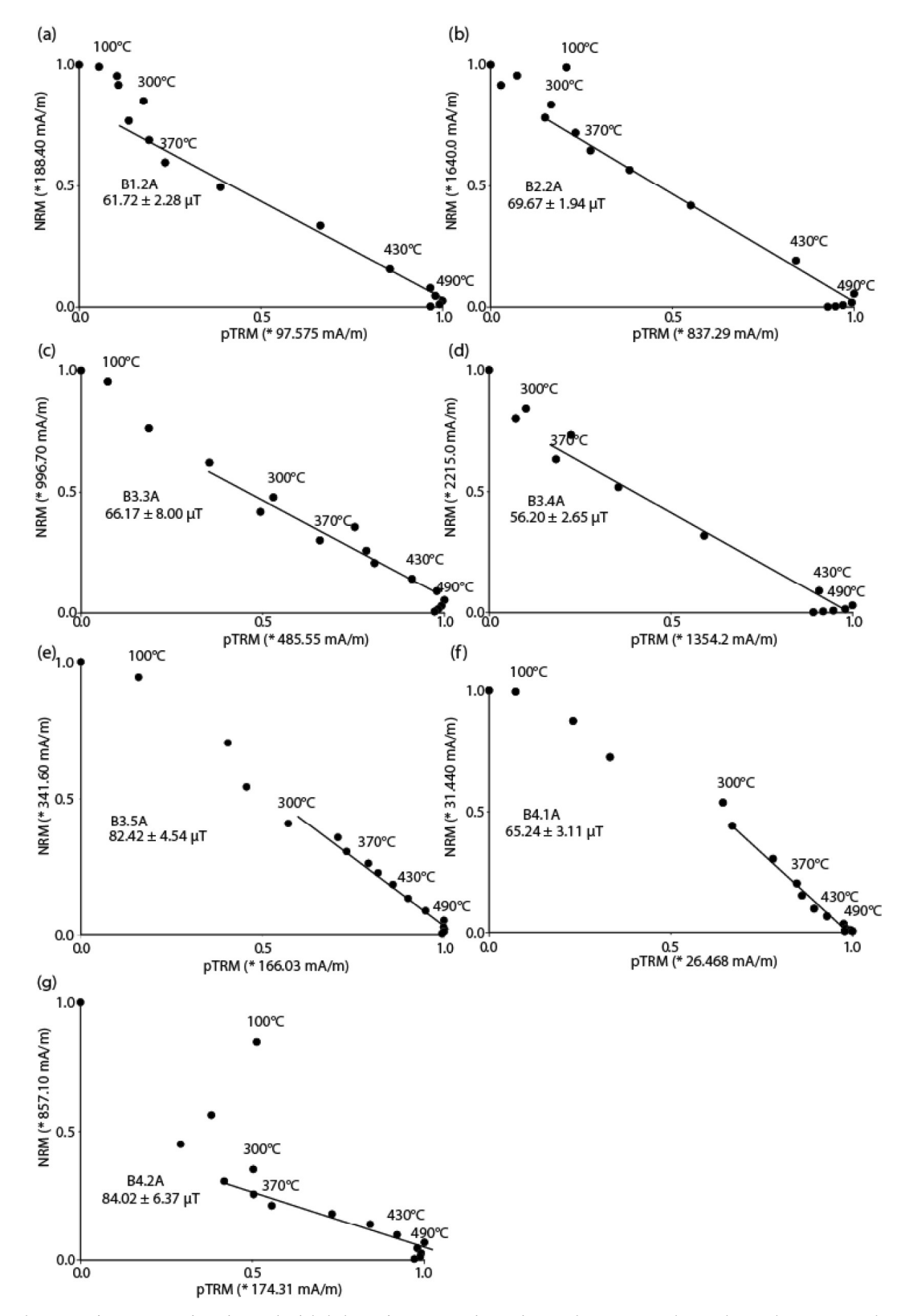


Fig. 7. Arai-type diagrams of NRM-pTRM for sub-samples labeled "A", from a) sample 1.2, b) sample 2.2, c) sample 3.3, d) sample 3.4, e) sample 3.5, f) sample 4.1, and g) sample 4.2. Note that sample B4.2A was rejected in obtaining the mean intensity.

five vitrified samples (Fig. 6b) is more likely to represent the TRM recorded at the time of the hillfort vitrification, and will be used to compare with paleointensity and geomagnetic field models.

Moreover, given the steep inclination of these directions, which is due to the high latitude of the study area, calculations of inclinationonly mean directions, using the method of Arason and Levi (2010), were made. The inclination-only mean for the five most-vitrified samples is I = 74, k = 102, α_{95} = 7.5°, which will be the preferred inclination-only mean for the field recorded during vitrification. For comparison, the inclination-only mean of all samples is I = 73,

 $k=101,\,N=7,\,\alpha_{95}=6^\circ.$ Overall, although an inclination-only mean may provide a smaller uncertainty for high-latitude directions, the small sample size remains the predominate control on the radius of 95% confidence for these directions.

3.4. Paleointensity

The results of the paleointensity experiments from chips taken on seven of the eight oriented cores (i.e., all but sample 2.1) were, overall, very consistent. Arai-type diagrams (Fig. 7), produced using Thellier-Tool to plot the pTRM with respect to the remanence remaining at every thermal double step, indicate the following. Between $\sim 300\text{--}500~^\circ\text{C}$ there is a linear relationship between primary remanence decay and TRM gain, which allows an estimate of the paleofield intensity for each specimen to be determined. Similar temperature ranges (i.e., 5–12 pairs of steps from 200 to 530 $^\circ\text{C}$, and exceptionally for sub-sample B4.2B starting at 120 $^\circ\text{C}$, see Table 2) defined linear segments on the Arai-type plots (Fig. 7), and were used to determine the estimated paleofield for each sample.

The experiments conducted for the first set of sub-samples (labelled as "A" on Table 2) did not include pTRM checks. However, the good linear fits in the Arai-type plots are of good quality (i.e., an "a" rating using the quality criteria specified in Table S.6 and calculated with ThellierTool; see also Coe et al. (1978) and Selkin and Tauxe (2000) for details). This data quality, with no pTRM checks, is mainly determined by the number of measurement steps and the linear regression statistics for the Arai-type plot. In addition, the reversibility of the thermomagnetic curves, and lack of change in low-field susceptibility measured after each heating step, suggest that these results are not likely influenced by alteration of the magnetic phases during these experiments.

For the additional five chip samples that were selected for experiments including pTRM in-field and tail checks (labelled as "B" on Table 2), results were corrected for these alteration checks as allowed by ThellierTool when the procedures by Valet et al. (1996) and Leonhardt et al. (Leonhardt et al., 2004; Leonhardt et al., 2003) are applied (Fig. 8, 'pTRM corrected calc' on Table 2). These data indicate that the revised experiments were for the most part successful, with class B or class A results (using the standard quality criteria in Thellier Tool, Table S.6). The results from a second chip of vitrified material from sample 4-2 (B4-2B) indicated possible influence of PSD-MD behavior, and had a paleointensity result that was significantly different than that obtained from the first set of results. For the other set of four samples, the paleointensity values before and after correction of the pTRM checks were similar (difference in values less than 8 μ T). Table 2 lists the obtained intensities, corresponding error values, and ThellierTool quality rating for the measured samples (see Table S.6 for additional information about the quality criteria selected in the paleointensity results analysis).

The results from both sets of experiments yield similar estimates of the paleointensity recorded by these samples. For the first set of non-pTRM checked data (labeled "A"), the mean intensity is $67.8 + /-7.3 \, \mu T$ (Mean-Set A on Table 2, after excluding the non-vitrified sample 4.2, which exhibited a less well-determined paleointensity, a relatively large value of error in the best fit line, and a multi-component vector behavior in the thermal demagnetization of the NRM). For the second set of pTRM-checked data (labeled "B"), the mean of all five samples after using the pTRM checks for corrections is $64.4 + /- 6 \, \mu T$ (Mean-Set B on Table 2, considering all Set B in this case). The relatively close correspondence between the paleointensities from the pTRM-checked data (Set B) and the set for which no pTRM checks were conducted (Set A) suggests that both groups of results yield reliable estimates of geomagnetic field paleointensity.

We also note that bias in cooling rates (large differences between the rates of cooling in laboratory settings during the pTRM experiments and the rate of cooling of the artifacts or material being studied) can result in a bias for the paleointensity determination (Ferk et al., 2010). Nevertheless, for the vitrified materials of Borborg (and other) hillforts, the mechanism of melting, including the duration of heating and cooling, is not well known. Therefore, an attempt to correct paleointensity values for cooling rates requires further study and experiments that are outside the scope of this present initial study.

4. Discussion

The mean direction from the well-vitrified samples (Fig. 6b) is D = 11.3, I = 73.7, N = 5, k = 115, $\alpha_{95} = 7.2^{\circ}$, and was used for a comparison with models for paleosecular variation. The preferred paleointensity value, after considering quality criteria, is a combined mean of the results obtained from the well-vitrified sub-samples in Table 2 (i.e., B1-2A, B1-2B, B2-2A, B3-3a, B3-3B, B3-4A, B3-4B and B3-5A; results in italic on Table 2), equal to 67.9 \pm -6.4 μ T. For this comparison, the regional archaeomagnetic field model for Europe, SCHA.DIF.3 K (Pavón-Carrasco et al., 2009), with data and MatLab script updates from 2015, are used. The regional field model was selected as it should account for prevalent zonal characteristics of the geomagnetic field for the region in which these Iron Age hillforts are common, and so would better serve as a better reference than a global field model. For a more refined testing, an additional comparison with ARCH 3 K.1 model (Korte et al., 2009) is also included in Fig. S.7.1. For further reference, additional comparisons were made using the regional model (SCHA.DIF.3 K) using only the paleointensity, and using mean inclination and paleointensity. Those results are in section S.7 of the Supplementary Material.

Given the relatively small number of samples for both the directional and paleointensity results, the error estimates for the mean direction and paleointensity introduce relatively large error-ranges in the probability-density function used to determine the best-fit age estimates. For the comparison with the SCHA.DIF.3 K model, 95% confidence intervals were used for the age determination. The dating graphs are shown in Fig. 9. The model values for declination, inclination, and field intensity for the Broborg site, with ages ranging from 0 CE to 1300 CE are plotted (Fig. 9, red curves) and compared with the observed paleomagnetic declination, inclination, and intensity (Fig. 9, blue lines with confidence intervals in green). The probability density diagram at 95% confidence for each value of declination, inclination and intensity, is shown in the middle panel in Fig. 9. The combined probability density functions of declination-inclination-intensity at 95% confidence are shown in the bottom panels of Fig. 9.

Over the age range we chose to evaluate due to archaeological constraints, there are several time intervals that are identified as possible ages for the Broborg vitrification. At 95% confidence, these are 0–82 CE, 389–579 CE, 602–752 CE, and 965–1300 CE. The ages from 389 to 579 CE (95% confidence) agree well with the wood-post ¹⁴C age discussed above. The oldest range and the youngest range do not match well with the known archeological context of the site.

Several new ¹⁴C ages have been determined for the site during the 2017 round of excavations, of which the collection of these samples for paleomagnetic dating was a part (Englund, 2018). The most reliable dates come from the so-called "activity layer" [#A506 in (Englund, 2018)] which is deposited along the side of the wall and must be contemporaneous with, or after, the vitrification event, particularly since in some areas the archaeological context of this layer is overlaying part of the vitrified wall. Three reliable dates from charcoal hardwood (possibly oak), charred grain shells, and charred oat, respectively, give 95.4% probability (2 sigma calibration) of 420–590 CE, 410–560 CE, and 420–580 CE (Englund, 2018). These dates are indirect dating of the wall of course. No adequate charcoal was obtainable within the wall for dating.

The vitrified material used to obtain paleodirection and paleointensity were not collected in the same part of the wall as the trench excavation (see Fig. 1c), because no suitable highly glassy massive

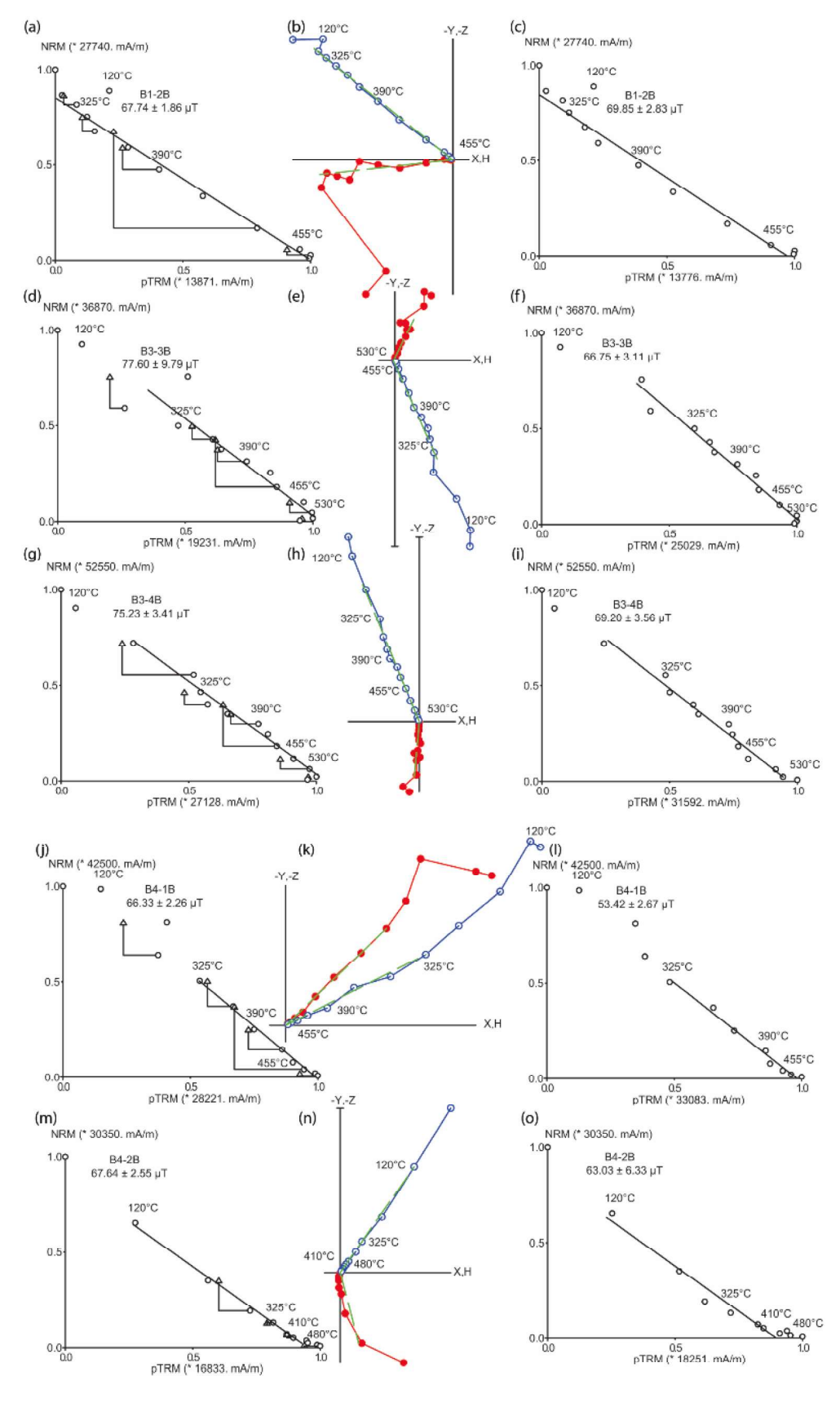


Fig. 8. Paleointensity results from second set of analyses (labeled "B"), which included pTRM checks. For each small chip sample, Arai-type diagrams with pTRM checks indicated are shown on left column, orthogonal vector plot for thermal demagnetization of NRM (note these samples are not oriented) with ChRM indicated by dashed green line shown in the center column, and Arai-type diagram corrected for pTRM checks using ThellierTool shown on the right hand column. (a-c) are for vitrified sample B1-2b, (d-f) are for vitrified sample B3-3b, (g-i) are for vitrified sample B3-4b, (j-l) are for chip of vitrified material from heated sample B4-1b, and (m-o) are for a chip of vitrified material from heated sample B4-2b.

material was obtainable in the trench area. However, assuming that all the sections of the wall were vitrified in the same generation of inhabitants, the 389–579 CE paleomagnetic date range (obtained in this work) agrees well with the ¹⁴C ages. It is also possible, however, that

the vitrified wall sampled for paleomagnetic dating was heated later, and the 602–752 CE date is accurate.

Unfortunately, given the difficulties in obtaining properly vitrified standard oriented samples, it is unlikely that the current data can

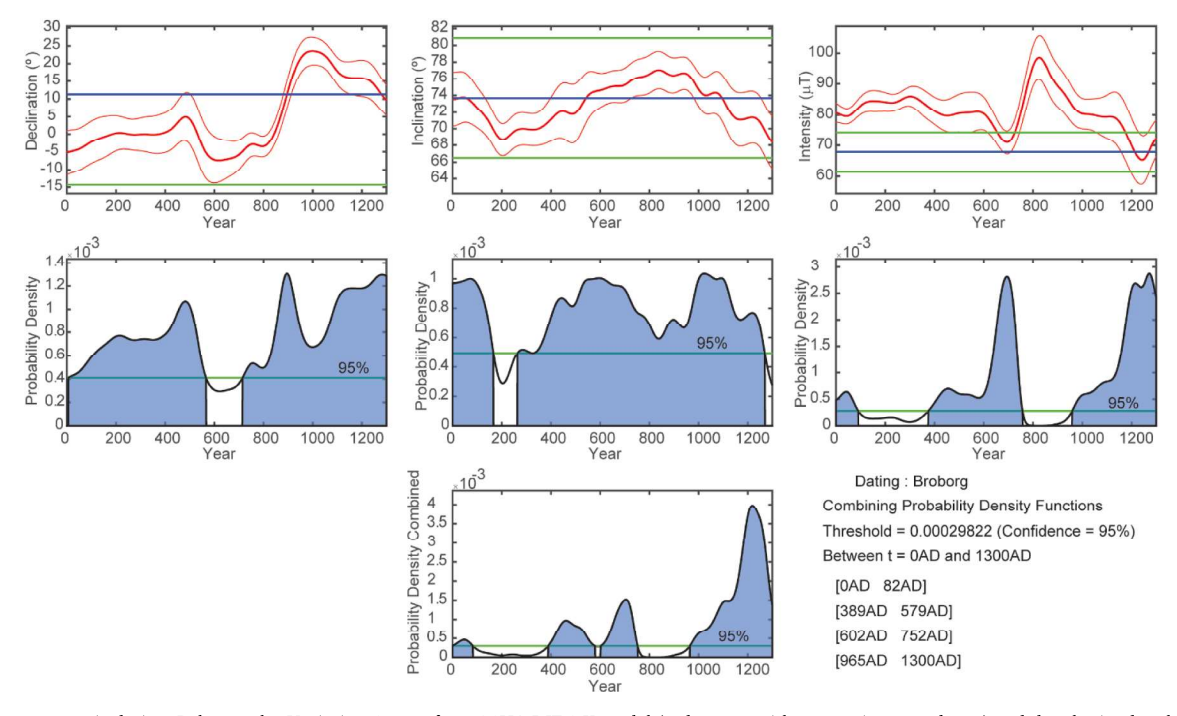


Fig. 9. Archaeomagnetic dating. Paleosecular Variation Curves from SCHA.DIF.3 K model (red curves with uncertainty envelopes) and the obtained archaeomagnetic declination, inclination, and intensity data (blue lines with green uncertainty lines). The middle graphs show probability density functions shaded for significant matches between data and model at 95% confidence (green line). Combined probability density functions for declination-inclination-intensity are shown in the bottom panel at 95% confidence, with the most probable dates shown in brackets.

distinguish between a whole site vitrification in the early 400 s versus either a progressive site vitrification for a few hundred years, or episodes of vitrification that took place during both the 389–579 CE and 602–752 CE time intervals. An alternate approach for such sites may be suggested by the paleointensity data, which were obtained from unoriented small chips of vitrified material from the cores, demonstrating that a reliable paleointensity estimate can be obtained even in a small portion of material. A larger number of chip samples could be more easily collected from sites in those conditions, and so more precise estimates of the age(s) of hillfort vitrification events could be attempted from paleointensity measurements alone. For comparison, a dating model constrained with only the Broborg paleointensity data is given in the Supplementary Material, showing that it gives similar results to the overall model.

5. Conclusions

The combined petrographic, rock-magnetic, and paleomagnetic analyses of vitrified material from the Broborg hillfort indicates that the melt products are very good recorders of the geomagnetic field, and that the paleofield direction and intensity together have very good potential to directly date the age of vitrification of these structures. The similarity of directions obtained from the vitrified material from different portions of the hillfort may suggest that the vitrification present in the structure (or at least the portions sampled for this work) occurred during the same time period. A comparison with regional models of geomagnetic field direction and intensity and the observed paleomagnetic directions and paleofield intensity can be used to constrain the age of the vitrification event. The precision of this age estimate could be markedly improved by collecting a modest number of additional samples. Given the utility of the paleointensity measurements, and the smaller unoriented samples required for these measurements, it may be possible to even better constrain different parts of vitrified hillfort structures in the future using these techniques.

CRediT authorship contribution statement

Mostafa Ahmadzadeh: Investigation, Software, Writing - original draft, Writing - review & editing. Cristina García-Lasanta: Data curation, Investigation, Software, Validation, Writing - original draft, Writing - review & editing. Bernard Housen: Formal analysis, Methodology, Resources, Supervision, Writing - review & editing. John S. McCloy: Conceptualization, Funding acquisition, Methodology, Project administration, Supervision, Writing - review & editing.

Declaration of Competing Interest

The authors declare that they have no known competing financial interests or personal relationships that could have appeared to influence the work reported in this paper.

Acknowledgements

The authors gratefully acknowledge all the members of the Broborg hillfort excavation team, including Rolf Sjöblom, Mia Englund, Erik Ogenhall, Eva Hjärthner-Holdar, Jamie Weaver, Carolyn Pearce, and Albert Kruger. The authors especially thank Jack Clarke for assistance with the field sample collection and William Callebert for assistance in collecting the paleodirection data. The authors thank the US Department of Energy Office of River Protection for funding through 89304017CEM000001, and Roger Edenmo, the County authority in Sweden, for permission to take samples. Preliminary measurements were taken at the Institute for Rock Magnetism at the University of Minnesota (funded by the Earth Sciences Instrumentation and Facilities program of the National Science Foundation) and the authors thank Joshua Feinberg for his help. This paper was substantially improved from the detailed and thoughtful comments of two anonymous reviewers.

Appendix A. Supplementary data

Supplementary data to this article can be found online at https://doi.org/10.1016/j.jasrep.2020.102311.

References

- Arason, P., Levi, S., 2010. Maximum likelihood solution for inclination-only data in paleomagnetism. Geophys. J. Int. 182, 753–771.
- Berrocal-Rangel, L., García-Giménez, R., Ruano, L., Vigil de la Villa, R., 2019. Vitrified Walls in the Iron Age of Western Iberia: New Research from an Archaeometric Perspective. Eur. J. Archaeol. 22, 185–209.
- Brothwell, D.R., Bishop, A.C., Woolley, A.R., 1974. Vitrified forts in Scotland: A problem in interpretation and primitive technology. J. Archaeol. Sci. 1, 101–107.
- Catanzariti, G., McIntosh, G., Monge Soares, A.M., Díaz-Martínez, E., Kresten, P., Osete, M.L., 2008. Archaeomagnetic dating of a vitrified wall at the Late Bronze Age settlement of Misericordia (Serpa, Portugal). J. Archaeol. Sci. 35, 1399–1407.
- Clelland, S.-J., 2011. Developing Archaeomagnetic Dating in the British Iron Age. University of Bradford, Archaeological Sciences, PhD.
- Coe, R.S., 1967. Paleo-intensities of the Earth's magnetic field determined from Tertiary and Quaternary rocks. J. Geophys. Res. 1896–1977 (72), 3247–3262.
- Coe, R.S., Grommé, S., Mankinen, E.A., 1978. Geomagnetic paleointensities from radiocarbon-dated lava flows on Hawaii and the question of the Pacific nondipole low. J. Geophys. Res. Solid Earth 83, 1740–1756.
- Cotton, M.A., 1954. British Camps with Timber-Laced Ramparts. Archaeol. J. 111, 26–105.
- Deer, W.A., Howie, R.A., Zussman, J., 1992. An introduction to rock-forming minerals. Longman, Essex, England.
- Englund, M., 2018. Broborg Hillfort. A Research Study of the Vitrified Wall. Report 2018:103, The Archaeologists, The National Historical Museums, Stockholm.
- Fagerlund, D., 2009. Fornborgen Broborg. Arkeologiska undersökningar 1982 och 1983. rapporter 2009:05, Upplandsmuseets, Uppsala.
- Fisher, R., 1953. Dispersion on a Sphere. Proceedings of the Royal Society of London. Series A, Mathematical and Physical Sciences, 217, 295–305.
- Ferk, A., Aulock, F.W.v., Leonhardt, R., Hess, K.U., Dingwell, D.B., 2010. A cooling rate bias in paleointensity determination from volcanic glass: An experimental demonstration. J. Geophys. Res. Solid Earth 115, B08102.
- Gentles, D.S., 1989. Archaeomagnetic Directional Studies of Large Fired Structures in Britain. Department of Geological SciencesPolytechnic, PhD, Plymouth.
- Britain. Department of Geological SciencesPolytechnic, PhD, Plymouth. Gentles, D., Tarling, D.H., 1993. Vitrified forts archaeomagnetic dating. Curr. Archaeol. 133, 18–22.
- Harding, D., 2012. Iron Age Hillforts in Britain and Beyond. Oxford University Press,
- Harrison, R.J., Feinberg, J.M., 2008. FORCinel: An improved algorithm for calculating first-order reversal curve distributions using locally weighted regression smoothing. Geochem. Geophys. Geosyst. 9, Q05016.
- Kirschvink, J.L., 1980. The least-squares line and plane and the analysis of palaeomagnetic data. Geophys. J. R. Astron. Soc. 62, 699–718.
- Korte, M., Donadini, F., Constable, C.G., 2009. Geomagnetic field for 0–3 ka: 2. A new series of time-varying global models. Geochem. Geophys. Geosyst. 10, Q06008.
- Kresten, P., 2004. The Vitrified Forts of Europe: Saga, Archaeology, and Geology. In: Pecchio, M. (Ed.), International Council for Applied Mineralogy: development in Science and Technology. ICAM-BR, São Paulo, pp. 355–357.
- Kresten, P., Ambrosiani, B., 1992. Swedish vitrified forts a reconnaisance study. Fornvännen Journal of Swedish Antiquarian Research 87, 1–17.
- Kresten, P., Goedicke, C., Manzano, A., 2003. TL-Dating of Vitrified Material. Geochronometria – J. Methods Appl. Absolute Chronol. 22, 9–14.
- Kresten, P., Kero, L., Chyssler, J., 1993. Geology of the vitrified hill-fort Broborg in Uppland, Sweden. Geol. Fören. Stockh. Förh. 115, 13–24.

- Kresten, P., Kresten, F., 1996. Hill-forts with vitrified or calcined ramparts: Index and reference list. Geoarchaeological Laboratory (GAL), the Central Board of National Antiquities. Department of Archaeological Excavations, Uppsala, Sweden.
- Lattard, D., Engelmann, R., Kontny, A., Sauerzapf, U., 2006. Curie temperatures of synthetic titanomagnetites in the Fe-Ti-O system: Effects of composition, crystal chemistry, and thermomagnetic methods. J. Geophys. Res.: Solid Earth 111, B12S28.
- Leonhardt, R., Heunemann, C., Krása, D., 2004. Analyzing absolute paleointensity determinations: Acceptance criteria and the software ThellierTool4.0. Geochem. Geophys. Geosyst. 5, Q12016.
- Leonhardt, R., Matzka, J., Menor, E.A., 2003. Absolute paleointensities and paleodirections of miocene and pliocene lavas from Fernando de Noronha, Brazil. Phys. Earth Planet. Inter. 139, 285–303.
- Lurcock, P.C., Wilson, G.S., 2012. PuffinPlot: A versatile, user-friendly program for paleomagnetic analysis. Geochem., Geophys., Geosyst. 13, Q06Z45.
- Pavón-Carrasco, F.J., Osete, M.L., Torta, J.M., Gaya-Piqué, L.R., 2009. A regional archeomagnetic model for Europe for the last 3000 years, SCHA.DIF. 3K: Applications to archeomagnetic dating. Geochem. Geophys. Geosyst. 10, Q03013.
- Ralston, I., 1986. The Yorkshire Television vitrified wall experiment at East Tullos, City of Aberdeen District. Proceedings of the Society of Antiquaries of Scotland 116, 17–40.
- Ralston, I., 2013. Celtic Fortifications. The History Press, Stroud, Gloucestershire. Riisager, P., Riisager, J., 2001. Detecting multidomain magnetic grains in Thellier pa-
- Riisager, P., Riisager, J., 2001. Detecting multidomain magnetic grains in Thellier palaeointensity experiments. Phys. Earth Planet. Inter. 125, 111–117.
- Roberts, A.P., Almeida, T.P., Church, N.S., Harrison, R.J., Heslop, D., Li, Y., Li, J., Muxworthy, A.R., Williams, W., Zhao, X., 2017. Resolving the Origin of Pseudo-Single Domain Magnetic Behavior. J. Geophys. Res. Solid Earth 122, 9534–9558.
- Röpke, A., Dietl, C., 2014. The vitrified Bronze Age fortification of Bernstorf (Bavaria, Germany) an integrated geoarchaeological approach. European Geologist 38, 25–32.
- Russell, M., 1894. The vitrified forts of the North of Scotland. Journal of the British Archaeological Association 50, 205–222.
- Sanderson, D.C.W., Placido, F., Tate, J.O., 1985. Scottish vitrified forts: Background and potential for TL dating. Nuclear Tracks and Radiation Measurements (1982), 10, 799–809
- Selkin, P.A., Tauxe, L., 2000. Long-term variations in palaeointensity. Philosophical Transactions of the Royal Society of London. Series A: Mathematical, Physical and Engineering Sciences 358, 1065–1088.
- Thellier, E., Thellier, O., 1959. Sur l'intensité du champ magnétique terrestre dans le passé historique et géologique. Annales de Geophysique 15, 285–378.
- Torsvik, T.H., Briden, J., Smethurst, M., 2000. Super IAPD Interactive Analysis of Paleomagnetic Data, software, available http://www.earthdynamics.org/software/IAPD2016.zip.
- Valet, J.-P., Brassart, J., Le Meur, I., Soler, V., Quidelleur, X., Tric, E., Gillot, P.-Y., 1996. Absolute paleointensity and magnetomineralogical changes. J. Geophys. Res. Solid Earth 101, 25029–25044.
- Vernioles, J.D., 2013. Les Sites Vitrifiés de France: Inventaire et mode de réalisation. In: Docteur en Archéologie. Université.
- Verwey, E.J.W., 1939. Electronic conduction of magnetite (Fe₃O₄) and its transition point at low temperatures. Nature 144, 327–328.
- Weaver, J.L., Pearce, C.I., Sjöblom, R., McCloy, J.S., Miller, M., Varga, T., Arey, B.W., Conroy, M.A., Peeler, D.K., Koestler, R.J., DePriest, P.T., Vicenzi, E.P., Hjärthner-Holdar, E., Ogenhall, E., Kruger, A.A., 2018. Pre-Viking Swedish hillfort glass: a prospective long-term alteration analogue for vitrified nuclear waste. Int. J. Appl. Glass Sci. 9, 540–554.
- Yoder Jr., H.S., Tilley, C.E., 1962. Origin of basalt magmas: an experimental study of natural and synthetic rock systems. J. Petrol. 3, 342–532.
- Youngblood, E., Fredriksson, B.J., Kraut, F., Fredriksson, K., 1978. Celtic vitrified forts: Implications of a chemical-petrological study of glasses and source rocks. J. Archaeol. Sci. 5, 99–121.
- Zijderveld, J.D.A., 1967. AC demagnetization of rocks: Analysis of results. In: Collinson, D.W., Creer, K.M., Runcorn, S.K. (Eds.), Methods in Paleomagnetism. Elsevier, pp. 254–286.